Check for updates

Received: 26 October 2020 | Revised: 16 December 2020 | Accepted: 17 December 2020

DOI: 10.1002/ppap.202000218

FULL PAPER

PLASMA PROCESSES AND POLYMERS

A novel Deal–Grove-inspired model for fluorine-based plasma jet etching of borosilicate crown optical glass

Faezeh Kazemi[1] | Georg Boehm[1] | Thomas Arnold[1,2]

[1]Leibniz Institute of Surface Engineering (IOM), Leipzig, Germany

[2]Institute of Manufacturing Science and Engineering, Faculty of Mechanical Science and Engineering, Technische Universität Dresden, Dresden, Germany

Correspondence
Faezeh Kazemi, Leibniz Institute of Surface Engineering (IOM), Permoserstraße 15, 04318 Leipzig, Germany.
Email: faezeh.kazemi@iom-leipzig.de

Funding information
German Federal Ministry of Education and Research (BMBF) within the framework of the InnoProfile-Transfer, Grant/Award Number: 03IPT706X

Abstract

The Deal–Grove model is a state-of-the-art approach proposed for describing the thermal oxidation of silicon and the oxide thickness over time. In this study, the Deal–Grove concept provided the inspiration for a mathematical model for simulating plasma jet-based dry etching process of borosilicate crown glass (N-BK7®). The whole process is contained in two so-called Deal–Grove parameters, which are extracted from experimental data including local etching depth and surface temperature distribution. The proposed model is extended for the evolution of dynamic etch profiles, and the obtained results are validated experimentally. By establishing such a model, it is possible to predict the effect of the residual layer and surface temperature on the evolution of local etching depths over dwell time.

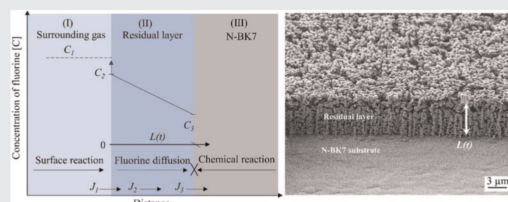

1 | INTRODUCTION

Plasma-assisted chemical etching techniques under atmospheric pressure are often used for machining of optical surfaces. Some examples of these techniques are plasma chemical vaporization machining,[1–5] reactive atom plasma,[6,7] atmospheric-pressure plasma processing,[8] arc-enhanced plasma machining technology,[9] and chemically reactive plasma jet machining (PJM).[10] Among them, PJM is commonly used for ultraprecision surface machining of optical glasses. Due to its atomistic material removal mechanism without the application of any significant mechanical forces, the method provides a high degree of flexibility regarding manufacturable surface shapes. Hence, PJM is predestined for freeform optics fabrication.[11] Determined and localized dry etching enables PJM to create freeform shapes on the optical surface almost defect-free and without any subsurface damage.[12]

Currently, freeform optical surfaces are extensively applied in illumination applications, for example, for controlling spatial light intensity distribution. For such applications, molded optics with medium precision are often used.[13]

This is an open access article under the terms of the Creative Commons Attribution License, which permits use, distribution and reproduction in any medium, provided the original work is properly cited.
© 2020 The Authors. *Plasma Processes and Polymers* published by Wiley-VCH GmbH

With increasing miniaturization and ongoing downscaling of optical systems, more complex freeform surface designs with a higher degree of precision are gaining increasing importance.[14–16] Manufacturability and fabrication efficiency are often a limiting factor when specialized individual optical elements or low lot sizes are to be produced by mechanical abrasive techniques such as grinding and subaperture polishing.[17] Here, a processing chain[12] including PJM steps comes into play, as it has been shown to be able to efficiently fabricate precise freeform surfaces.[10,11]

During PJM, surface etching of the substrate is performed by plasma-generated fluorine atoms that penetrate a boundary layer located on the top of the treated surface and subsequent chemical reactions with the components of N-BK7. The chemical phenomena, such as adsorption of reactants, surface reactions, and product desorption, leading to the etched surface occur at the solid surface. Depending on the respective chemical components of the substrate material, reaction products with fluorine atoms can be either in a gaseous state, such as SiF_4 or BF_3, or in solid states, for example, NaF or KF. If reaction products are solid, they remain on the surface, forming a residual layer, otherwise, they desorb through the boundary layer to be exhausted. In the first case, the resulting residual layer strongly influences the ongoing etching process. As the interaction zone of the plasma jet and the surface is characterized by rotationally symmetric distribution functions describing the lateral concentration of reactive species and the surface temperature,[18] the resulting etch depth profile and residual layer profile also show a rotationally symmetric functional form. In a previous work, it was shown that the application of a PJM process to borosilicate crown glass N-BK7 using a fluorine-containing plasma jet creates partially nonvolatile metal fluoride by-products on the treated surface.[19] The progressive growth of the residual layer is observed for the increased etching time, leading to the inhibition of the etching. Understanding the spatiotemporal behavior of the etching process and the ability to predict the local etching rate function is a prerequisite to successful deterministic surface machining. However, due to various interactions at the N-BK7–plasma interface on the atomic level, deriving a physical model that includes all aspects in their complexity is challenging.

In this study, the well-known Deal–Grove (DG) model[20] was employed and modified to provide a useful framework to simulate the kinetics of the plasma etching process of N-BK7 for a wide range of residual layer thickness. The DG model is a well-established model for thermal oxide growth that has been introduced in the middle of the 60s, and due to its simplicity, it is still frequently applied.[21] One reason for this simplicity is that the whole process is contained in two so-called DG parameters by which the growth kinetics can be described.

Here, the determination of appropriate DG model parameters is based on fitting the local etching depth data that were experimentally obtained from static footprint etching. Additionally, local surface temperature data were used in the fitting procedure. After parametrizing, the model was extended to simulate etch profiles occurring in dynamic etching where the plasma jet is moved over the surface.

By evaluating lateral distributions of the residual layer and etching depths, the modeled local depth distribution was proved to be equivalent to the thickness of the corresponding residual layer. The obtained simulation results are validated experimentally for the case of dynamic etching processes. By establishing such a model, it is possible to consider the effect of the residual layer and surface temperature on the evolution of etching depths over dwell time. The obtained results lead to a better understanding of the plasma–surface interactions of N-BK7 and help to develop a predictable machining process for plasma-based freeform generation.

2 | DG MODEL

The DG model is used commonly to interpret and predict the thermal oxidation of silicon. It describes mathematically the growth of an oxide layer on the substrate surface. In particular, the model is largely used in semiconductor device fabrication.[22] The DG model explicitly considers three phenomena that the oxidizing species undergo during the process, including diffusion from the surrounding gas to the surface, diffusion through the existing oxide layer to the oxide–substrate interface, and interactions with the substrate (Figure 1). The concept of the DG model is based on two fundamental assumptions: (i) Fickian diffusion with a constant diffusion coefficient and (ii) linear dependence of the mobile oxidant

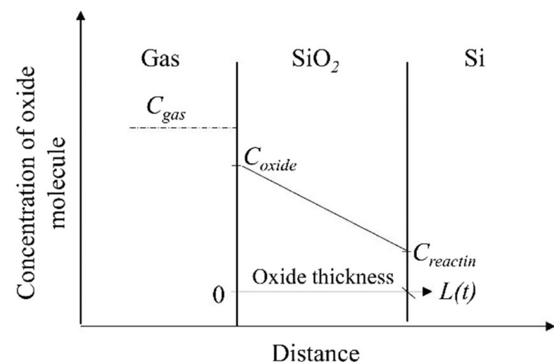

FIGURE 1 The one-dimensional Deal–Grove model used for the thermal oxidation of silicon[21]

concentration on its position in the oxide. On the basis of these assumptions, a linear parabolic function $L = (t)$ is obtained to illustrate the relation between oxide thickness L (nm) and oxidation time t (s). The linear term $L \sim t$ applies to extremely short oxidation times, leading to very thin oxide thicknesses, whereas the parabolic term $L \sim \sqrt{t}$ defines the growth at relatively large oxidation times. The DG model is applicable for single-crystal silicon under most conditions; however, empirical data indicate that very thin oxides (<25 nm) grow much more quickly in O_2 than that predicted by the model. This abrupt growth of the oxide layer is attributed to a reduction in oxidation kinetics, requiring a modification of the DG model. Nevertheless, the DG model provides precise results for thicker oxides if it is assumed that 25 nm of oxide exists instead of zero initial thickness (or any initial thickness <25 nm) before oxidation.

3 | MODELING OF PLASMA JET ETCHING OF N-BK7 WITH DG MODEL

As shown in our previous research work,[23] PJM of metal oxide-containing glass-like N-BK7 exhibits some limitations. Dry etching of N-BK7 using a fluorine-containing plasma jet creates partially nonvolatile metal-fluoride products developing a porous residual layer on the surface. A progressive growth of the residual layer is observed for an increased etching time t. Although after the process, the forming residual layer is removed easily by using a water-based solvent, it results in time-varying nonlinearity of the etching rate in the process. Hence, the application of fluorine-based reactive PJM to surface machining of N-BK7 is challenging and requires a comprehensive model to determine the time-varying nonlinearity of the material removal rate.[24] For this purpose, first, the exact interactions between plasma-generated active particles (i.e., fluorine) and the N-BK7 surface atoms should be clarified.

The principle of PJM of N-BK7 by fluorine-based plasma jet is shown in Figure 2.

Under this circumstance, the etching reactions continue at the interface between the formed residual layer and the substrate material, rather than the residual layer and the plasma discharge. During the etching process, three different phases that the plasma-generated etchant (i.e., fluorine) undergo can be recognized. Depending on species concentrations, material properties, and surface temperature T (°C) at any certain radial distance r (i.e., related to the symmetry axis of the rotationally symmetric plasma jet), the flux of fluorine atoms through each of the three phases can be expressed as follows (Figure 3):

I. Transmission from the surrounding gas atmosphere to the boundary layer of the N-BK7 surface, according to Henry's law, that is:

$$J_1 = h_1(C_1 - C_2), \tag{1}$$

where J_1 ($mol{\cdot}m^{-2}{\cdot}s^{-1}$) is the flux of fluorine in gas, h_1 ($m{\cdot}s^{-1}$) the gas-phase transport coefficient, C_1 ($mol{\cdot}m^{-3}$) the equilibrium concentration of the fluorine in the surrounding gas, and C_2 ($mol{\cdot}m^{-3}$) denotes the concentration of the

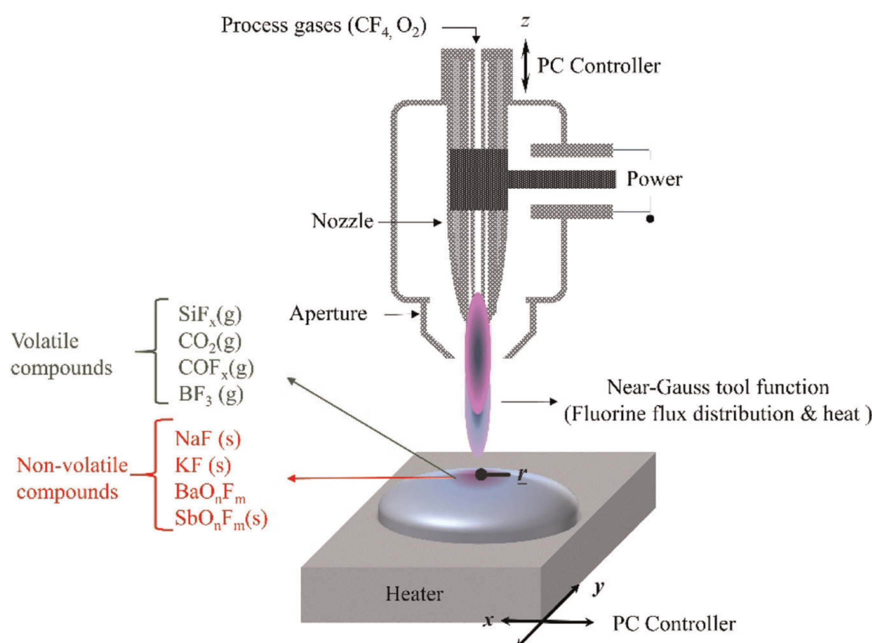

FIGURE 2 Fluorine-based plasma jet with the indicated zones of interest during interaction with N-BK7 surface

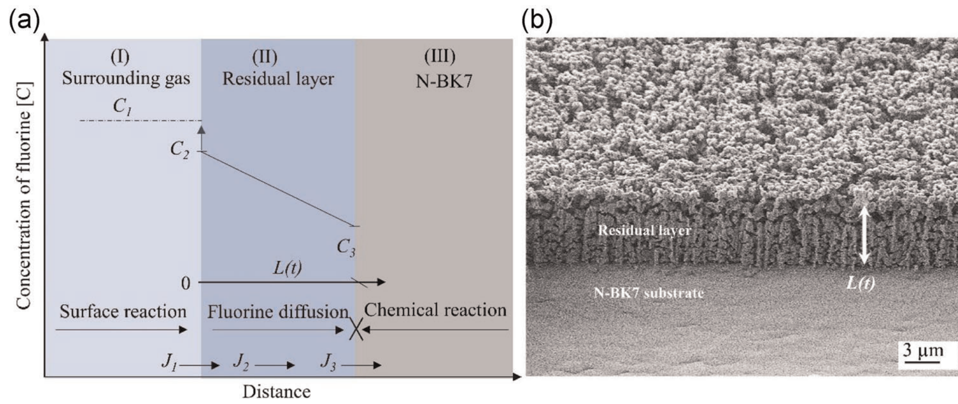

FIGURE 3 (a) Modeling plasma jet etching with the Deal–Grove model. (b) Scanning electron microscopy measurement illustrating the surface morphology and thickness of the residual layer after etching at an initial surface temperature $T_h = 350°C$

fluorine at the outer surface of the existing residual layer for absorbing inside a surface (surface reaction).

II. Diffusion through the existing residual layer to the layer–substrate interface, is based on Fick's law, that is:

$$J_2 = -D_2 \frac{dC}{dx} = D_2 \frac{C_2 - C_3}{L}, \tag{2}$$

where J_2 (mol·m^{-2}·s^{-1}) denotes the flux of fluorine in the residual layer, D_2 (m^2·s^{-1}) the effective diffusion coefficient, dC_2/dx the concentration gradient in the residual layer, C_3 (mol·m^{-3}) is the concentration of residual layer near the residue–substrate interface, and L is the residual layer thickness. The flux J_2 (mol·m^{-2}·s^{-1}) is derived on the basis of the assumed steady-state condition with $\partial J_2/\partial x = 0$, that is, no fluorine is reacting in the layer.

III. Reactions with the N-BK7 substrate: In the third part of the etching process, the flux of fluorine is consumed by the chemical reaction at the layer–substrate interface to further grow the residual layer and form volatile products. The reaction is considered as a first-order reaction, as it controls only the concentration of one reactant (i.e., fluorine). The rate law for such a reaction is given by the following:

$$J_3 = kC_3, \tag{3}$$

where J_3 (mol·m^{-2}·s^{-1}) is the flux of fluorine in reaction with the substrate material and k denotes the surface rate constant as the number of processes occurring at the residue–substrate interface. These processes may include dissociation of the fluorine molecule ($F_2 \rightarrow 2\,F$), Si–O or B–O bond breaking, and Si–F or B–F bond formation. The rate at which this reaction takes place should be proportional to the fluorine concentration at the interface C_3.

It is assumed that each of the phases proceeds at a rate proportional to the fluorine concentration. Due to similarities of the above-described phases of N-BK7 etching with thermal oxidation of silicon, the concept of the DG model is exploited here to model the PJM process of N-BK7 (Figures 1 and 3).

3.1 | Deriving the residual layer thickness

With the main assumption of the DG model, the above-described fluxes of fluorine are equal within the three different phases under steady-state conditions, that is:

$$J = J_1 = J_2 = J_3. \tag{4}$$

Then, by substituting C_2 and C_3 with C_1, it yields

$$J = \frac{kC_1}{1 + \frac{k}{h_1} + \frac{kL}{D_2}}. \tag{5}$$

The growth rate $R = dL/dt$ (m·s^{-1}) of the residual layer can be obtained directly from the ratio of the flux J and the concentration n (mol·m^{-3}) of reactant molecules (i.e., fluorine), forming a unit volume of the residual layer, that is:

$$R = \frac{dL}{dt} = \frac{J}{n} = \frac{1}{n} \frac{kC_1}{1 + \frac{k}{h_1} + \frac{kL}{D_2}}. \tag{6}$$

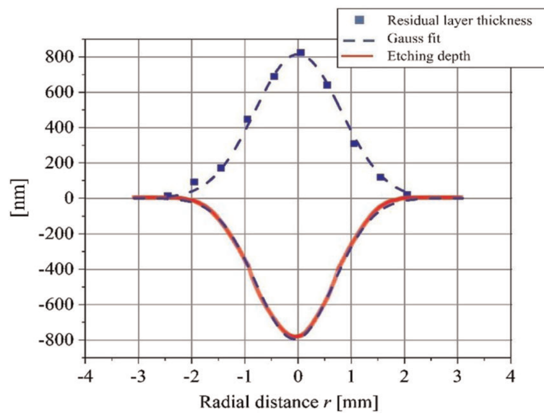

FIGURE 4 Profiles of the residual layer thickness (blue squares) and etching depth (red curve) after the removal of residual layer with water/ethanol obtained on the surface of N-BK7 using fluorine-based plasma jet at the initial temperature $T_h = 350°$ for etching time $t = 4$ s. The dashed lines are the corresponding Gaussian fits with amplitude $D_{max} \approx 800$ nm and $\sigma \approx 1.1$ mm

By defining the following parameters A (m) and B ($m^2 \cdot s^{-1}$) as

$$A = 2D_2\left(\frac{1}{k} + \frac{1}{h_1}\right), \quad (7)$$

$$B = \frac{2D_2C_1}{n}, \quad (8)$$

the differential Equation (6) can be rewritten as follows:

$$\frac{dL}{dt} = \frac{B}{A + 2L}. \quad (9)$$

3.2 | Analytical relationship of residual layer thickness and etching time

To obtain an analytical relationship between residual layer thickness L and etching time t, the first-order differential (9) must be solved. For this purpose, in the first step, the expression (9) can be rewritten as follows:

$$(A + 2L)\,dL = B\,dt. \quad (10)$$

By taking the integration of both sides of the expression (10), and with the assumption of an initial layer thickness L_0 (m) at $t = 0$ s, a quadratic equation is derived for the layer thickness L:

$$\int_{x_i}^{L}(A + 2L)\,dL = \int_0^t B\,dt, \quad (11)$$

$$L^2 + AL = B(t + \tau), \quad (12)$$

where parameter τ (s) is given by the following:

$$\tau = \frac{L_0^2 + AL_0}{B}. \quad (13)$$

Parameter τ takes into account any residual layer thickness at the start of the etching process. Solving Equation (12) for a given desired residual layer thickness L_0 results in the estimation of etching time t as follows:

$$t = \frac{L_0^2 - x_i^2}{B} + \frac{L_0 - x_i}{B/A}. \quad (14)$$

In this study, the initial layer thickness L_0 is assumed to be zero, as with this setting, acceptable results can be obtained.

However, solving the quadratic Equation (12) with respect to L leads to the following:

$$L = \frac{-A + \sqrt{A^2 + 4B(t + \tau)}}{2} = \left\{\begin{matrix} \frac{B}{A}(t + \tau) & t + \tau \ll \frac{A^2}{4B} \\ \sqrt{B(t + \tau)} & t + \tau \gg \frac{A^2}{4B} \end{matrix}\right\}, \quad (15)$$

where parameters B ($m^2 \cdot s^{-1}$) and B/A ($m \cdot s^{-1}$) are called the quadratic and linear rate constants, respectively.

3.3 | Derivation of local etching depth $D(t,T)$

According to our previous research,[23] once N-BK7 is sufficiently preheated to an initial temperature of 350°C, static etch profiles exhibit a Gaussian functional shape. Thus, in the first step, static footprint etchings were performed on preheated N-BK7 surfaces with $T_h = 350$°C to monitor the temporal evolution of the etch profiles. Afterward, the resulting layer thickness over the radial profile as well as the etching profile was measured. In this experiment, the plasma jet dwell time was adjusted to $t = 4$ s. The produced layer thickness cross-section was measured using a thin-film profiler, whereas the etching depth profile cross-section was determined by white light interferometry after removing the layer by rinsing the surface with water/ethanol.

As shown in Figure 4, the local etching depth D is equivalent to the thickness L of the residual layer, that is:

$$D(t) = L(t). \quad (16)$$

The plasma jet as a source of reactive species imposes a characteristic spatial distribution of fluorine flux on the surface, depending on the plasma parameters. Furthermore, according to our former investigation,[23,24] the heat flux of the plasma leads to the development of a spatio-temporal surface temperature distribution. Both effects lead finally to the characteristic bell-shaped

profiles of the residual layer thickness or etching depth, which can be approximated by a Gaussian function as follows:

$$D(r) = D_{\max} \exp\left(-\frac{r^2}{\sigma^2}\right). \tag{17}$$

Therefore, the variations of fluorine flux and temperature with the radial distance r must be considered in the model for simulation of local etching depths. Hence, the DG parameters B and B/A are a function of radial distance r and surface temperature $T(r,t)$. The local etching depth D can be expressed by one inclusive model equation as follows:

$$D(t, T(r,t), r) = \frac{-A(r, T(r,t)) + \sqrt{A^2(r, T(r,t)) + 4B(r, T(r,t))(t+\tau)}}{2}. \tag{18}$$

For the case of silicon oxidation, it was found experimentally[20,21] that the relation of model parameters B and B/A with temperature T can be well described by Arrhenius expressions. Therefore, it is assumed that the temperature dependence in the current case can be described by the Arrhenius expressions as follows:

$$B(r, T(r,t)) = \alpha_1(r) \exp\left(-\frac{E_{a1}}{k_B T(r,t)}\right), \tag{19}$$

$$\frac{B(r, T(r,t))}{A(r, T(r,t))} = \alpha_2(r) \exp\left(-\frac{E_{a2}}{k_B T(r,t)}\right), \tag{20}$$

where E_{a1} and E_{a2} denote the activation energy, k_B is the Boltzmann constant in eV, and $\alpha_1(r)$ ($m^2{\cdot}s^{-1}$) and $\alpha_2(r)$ ($m{\cdot}s^{-1}$) are the pre-exponential constants that are to be determined for the given radial distance r. A list of model parameters for the proposed DG model-based approach is presented in Table 1.

To find the model parameters $\alpha_1(r)$ ($m^2{\cdot}s^{-1}$) and $\alpha_2(r)$ ($m{\cdot}s^{-1}$), an estimation procedure based on fitting experimental data is proposed. To provide such data including local depth $D(r,t)$ and surface temperature $T(r,t)$, static etching was performed on a preheated surface with initial temperature $T_h = 350°C$ for different dwell times t, ranging from 1 to 60 s. The local etching depth and temperature data used for the fitting process are presented in Figure 5.

Then, by fitting the experimental data $D(r,t)$ and $T(r,t)$ for each individual radial distance r in expression (18), constants $\alpha_1(r)$ and $\alpha_2(r)$ and the activation energies E_{a1} and E_{a2} are determined. In this regard, it is required to solve nonlinear curve-fitting (data-fitting) problems in the least-squares sense that is implemented here by the MATLAB built-in function "lsqcurvefit."

The empirically estimated activation energy for fluorine-based plasma etching of fused silica (SiO_2) has been shown to be around 0.16 eV.[25,26] This activation energy usually is associated with the Si–O bond breaking process during SiO_2 removal process. However, compared with SiO_2, the activation energy of N-BK7 is expected to be less due to the presence of alkali metal ions (e.g., Na^+) in its glassy network. The results of the fitting process showed that the value of E_{a1} is very close to E_{a2}, and it can be set to the constant average value 0.05 eV. Moreover, our experiments revealed that the activation energy for N-BK7 is in the range of 0.03–0.06 eV. This result suggests that the origin of activation energies E_{a1} and E_{a2} is likely associated with the diffusion of fluorine through the residual layer and also with the interface chemical reaction rate (i.e., bond breaking process related to chemical reactions).

The results of fitting the experimental etching depth D to the DG model (18) are shown in Figure 6. According to Equation (8), parameters B and accordingly B/A are directly proportional to the flux of the fluorine (concentration C_1). Therefore, it is expected that the pre-exponential constants α_1 and α_2 adopt a bell-shaped functional form over the radial distance r as the distribution of fluorine flux follows a near-Gaussian shape.

Figure 7 shows the computed values of the pre-exponential functions $\alpha_1(r)$ and $\alpha_2(r)$ with respect to the radial distance r. With this parameter, the DG model can

TABLE 1 List of model parameters for the proposed Deal–Grove model-based approach

Model parameter (unit)	Description	Definition
B ($m^2{\cdot}s^{-1}$)	Quadratic term, a function of r and T	Equation (19)
B/A ($m{\cdot}s^{-1}$)	Linear reaction rate term, a function of r and T	Equation (20)
α_1 ($m^2{\cdot}s^{-1}$)	Pre-exponential constant of quadratic term	Estimated via fitting process at given r
α_2 ($m{\cdot}s^{-1}$)	Pre-exponential constant of linear reaction rate term	Estimated via fitting process at given r
E_{a1} (eV)	Activation energy in quadratic term	0.05
E_{a2} (eV)	Activation energy in linear reaction rate term	0.05

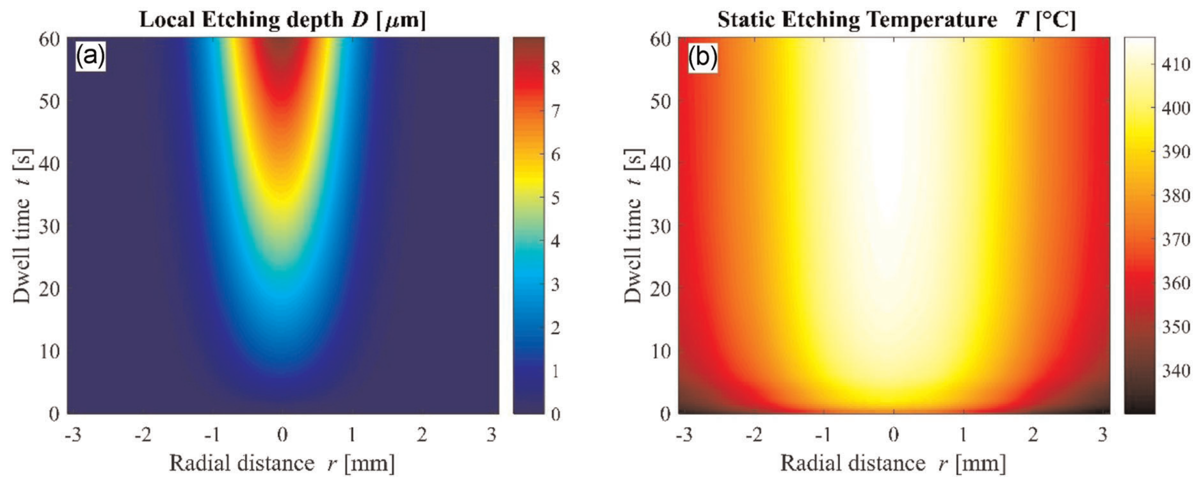

FIGURE 5 (a) Local etching depth $D(r,t)$ obtained by static etching at the initial temperature $T_h = 350°C$ after the removal of residual layer; (b) corresponding surface temperature distribution $T(r,t)$

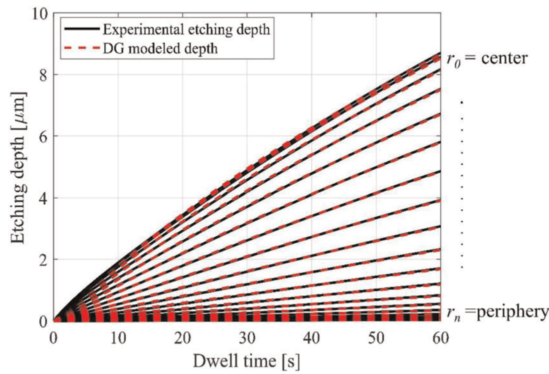

FIGURE 6 Results of fitting the experimental etching depth D to the Deal–Grove model (18) for exemplary values of radial distance r

be employed to model layer thickness or etching depth profiles for dynamic etching.

4 | MODELING OF DYNAMIC ETCHING

Whereas in the static case, the plasma dwells on a fixed position (e.g., for obtaining the material removal function), for the dynamic case, the plasma jet performs a motion relative to the surface along a prescribed path, for example, a raster path. In the case of static etching, for a given temperature distribution, the relation of local etching depth D and the dwell time t can be expressed as follows:

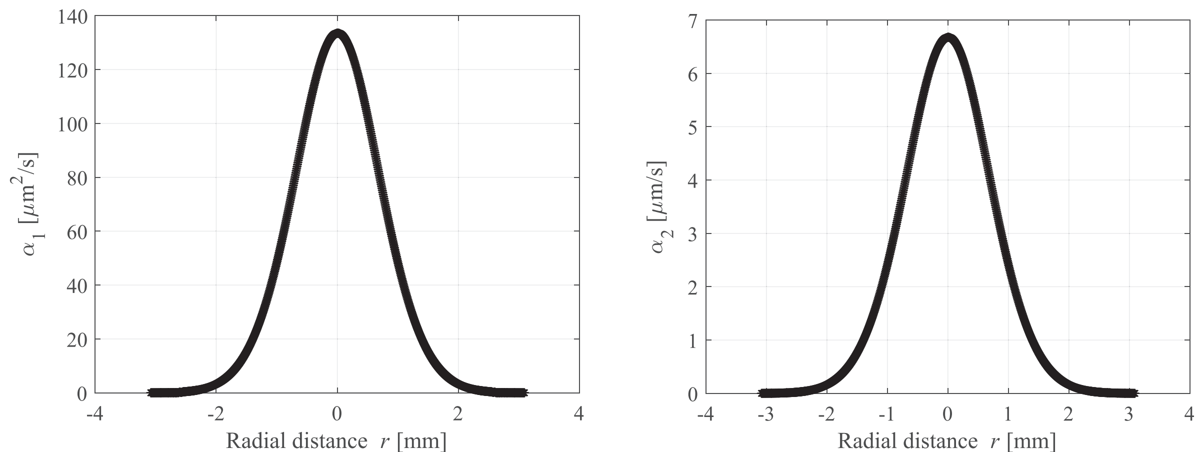

FIGURE 7 Pre-exponential functions $\alpha_1(r)$ and $\alpha_2(r)$ obtained for a range of radial distance r values using the fitting process on static etching experimental data

$$D = R_{\max}\, t \exp\left(-\frac{r^2}{\sigma^2}\right), \tag{21}$$

where $R_{\max}$ is the time-averaged maximum local etching rate.

To obtain a line etching as a simple case of dynamic machining, the plasma jet is horizontally moved in the y direction by a motion system, relative to the substrate surface, whereas the working distance is fixed. A straight line on the surface is then treated with a constant scan velocity v, resulting in a groove profile in the x direction that can be approximated by a Gaussian function. In this case, the local etching depth D for given scan velocity v can be obtained as follows:

$$D = N\int R_{\max} \exp\left(-\frac{(vt)^2 + x^2}{\sigma^2}\right) dt = \frac{N R_{\max}\, \sigma\sqrt{\pi}}{v} \exp\left(-\frac{x^2}{\sigma^2}\right). \tag{22}$$

Here, N is the number of line iterations. This equation expresses the convolution of the Gaussian rate function (21) with the constant dwell time distribution along the path in the y direction. The equivalent velocity v ($\mathrm{mm{\cdot}s^{-1}}$) for a certain dwell time t in the case of dynamic etching can be obtained when Equations (21) and (22) are set equal, with $x = r$, resulting in the relation:

$$v = \frac{\sigma(t)\sqrt{\pi}}{t}, \tag{23}$$

where $\sigma(t)$ is the standard deviation of the Gaussian function (i.e., a measure of the full width at half maximum [FWHM]) at the given dwell time t. For modeling line etching, parameters $\alpha_1(r)$ and $\alpha_2(r)$ found from static etching as well as the relevant surface temperature profiles obtained experimentally from dynamic line etchings $T(r,t)$ (not shown here) are inserted in Equation (18), and depth profiles are calculated, depending on the dwell time t.

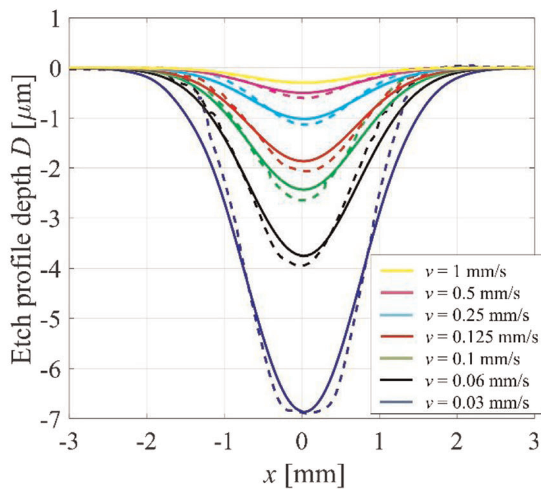

FIGURE 8 Etch profile depths obtained by experiments (dashed line) and the proposed Deal–Grove model (solid line) for line etching on N-BK7 surface with different scan velocities$v$

The corresponding scan velocity v can be estimated from Equation (23) for each modeled line etching profile by taking the respective $\sigma(t)$. The standard deviation $\sigma(t)$ is estimated by fitting the depth profile to a Gaussian function. Figure 8 shows the cross-section shapes of simulated depth profile and experimental results for line etching for different scan velocities. In general, the maximum depth of the modeled profiles agrees well with the experimental profiles. However, the modeled profiles exhibit slightly larger FWHM. This effect can be attributed to an overestimation of the etching depth, especially in the periphery of the profiles, as the model takes a two-dimensional temperature profile over the cross-section x into account. In other words, the surface temperature on a position x within the etched line is assumed to be constant. In the real experiment, the spatial temperature exhibits, however, a lateral distribution in the x, y plane that resembles a comet-like footprint, as shown, for example, in the study reported by Kazemi et al.[24] Thus, each position x experiences an increase of temperature up to the value taken in the model, and subsequently a decrease, when the plasma jet passes a certain position y. As the model disregards this temperature variation, the computed depth is larger than that observed in the experiment.

On the basis of experimental and DG-modeled etch profile depths of line etching provided in Figure 8, the maximum values of residual layer thickness (or equivalently the maximum etching depth) are calculated (Figure 9a). The maximum value of surface temperature for each corresponding scan velocity v is also shown. For the scan velocities v larger than $1.5\,\mathrm{mm{\cdot}s^{-1}}$ (i.e., dwell time $t < 1.1\,\mathrm{s}$), the residual layer thickness reveals the least dependence on scan velocity v; this behavior can be justified by a less pronounced variation of surface temperature.

For a deterministic process, the volumetric removal rate as an averaged value is often used to scale the tool function. As in the current case, the volumetric removal rate depends on time or velocity, respectively, it can be obtained from the integration of the individual depth profiles as follows:

$$\mathrm{VRR}(t) = v\int_{-\infty}^{+\infty} D(r,t)\, dr. \tag{24}$$

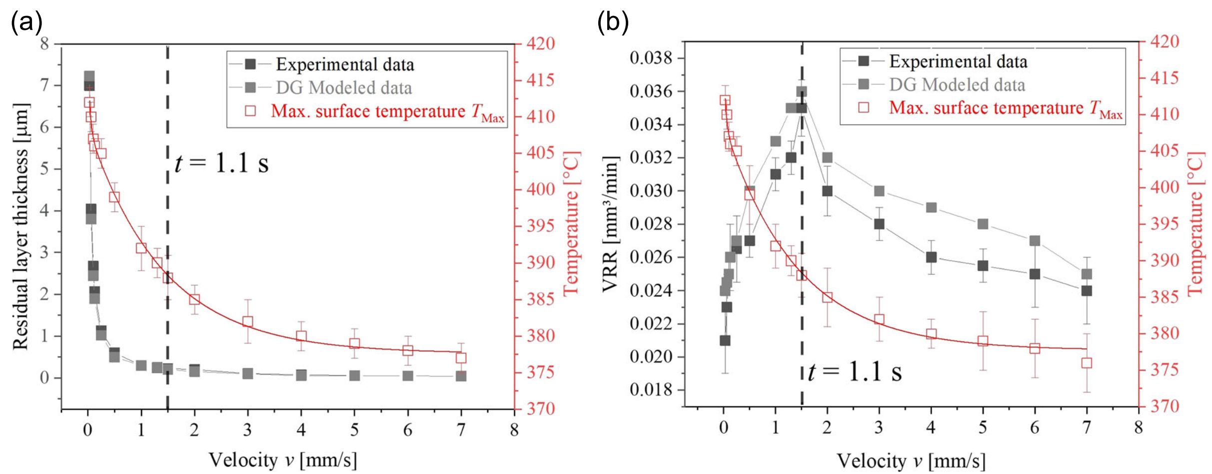

FIGURE 9 (a) Illustration of residual layer thickness and (b) volumetric removal rate (VRR) versus scan velocity obtained for the Deal–Grove-modeled and experimental line etching. The corresponding surface temperature is shown in the graphs as well

To calculate VRR values, numerical integration was performed for the DG-modeled and experimental etch profiles provided in Figure 8. The obtained results for different scan velocities v are presented in Figure 9b. With decreasing velocity, VRR increases and reaches the maximum value of $0.035\ mm^3 \cdot min^{-1}$ at $v = 1.5\ mm \cdot s^{-1}$ (i.e., $t = 1.1$ s). This behavior can be attributed to the effect of increasing surface temperature. However, as the scan velocity becomes $<1.5\ mm \cdot s^{-1}$ (i.e., $t > 1.1$ s), VRR converts to a decaying nonlinear function. Apparently, the scan velocity $v = 1.5\ mm \cdot s^{-1}$ can be regarded as a turning point where below this velocity, the growing residual layer reduces the etching rate and undermines the boosting effect of rising temperature. As shown in Figure 9b, this behavior is well predicted by the VRR values of the DG-modeled etch profiles.

The time-dependent VRR values of experimental and modeled etch profiles obtained from both static and line etchings (dynamic etching) are compared in Figure 10. The static etching shows higher values of VRR as compared with line etching due to its larger surface temperature distribution.

Noticeably, with an increase in the dwell time t (or decreasing scan velocity), on the one hand, the temperature rises, leading to a higher etching rate; on the other hand, the undesirable effect of residual layer thickness becomes more destructive. Experimental as well as modeled data for both line and static etching show that at low etching time $t < 1.1$ s (i.e., high scan velocity $v > 1.5\ mm \cdot s^{-1}$), the effect of surface temperature is dominant. However, at high etching time, the residual layer is thick enough to undermine the positive effect of temperature.

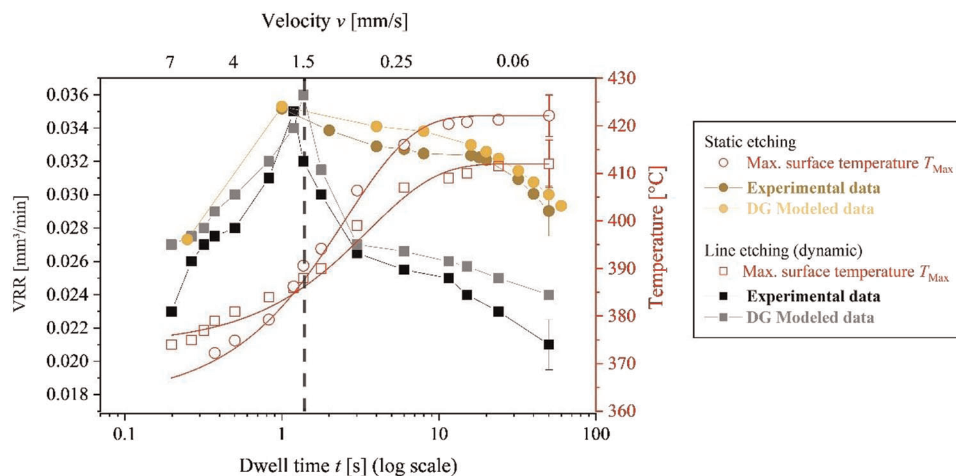

FIGURE 10 The time-dependent volumetric removal rate (VRR) of experimental and Deal–Grove-modeled etch profiles obtained from both static and line etchings. The corresponding surface temperature for static and dynamic etching is shown by red curves, respectively, with square and circle markers

The obtained results reveal that the proposed DG model approach can predict the effect of the residual layer as well as surface temperature on the evolution of etching depths over dwell time.

5 | CONCLUSION

The DG model is used commonly to describe mathematically the growth of an oxide layer on the surface of silicon. This model determines the relationship of oxide thickness with oxidation time, with very good approximation for oxide thicknesses of more than 23 nm.

Plasma jet etching of N-BK7 surface shows a complex behavior, as it creates partially nonvolatile metal-fluorine products developing a residual layer on the surface. The progressive growth of the residual layer is observed for increased etching time, leading to inhibition of local dry etching. Due to various chemical interactions at the N-BK7–plasma interface on an atomic level, deriving a physical model that includes all aspects in their complexity is literally challenging. In this paper, the DG model is exploited to interpret the interactions between plasma-generated active fluorine and the N-BK7 surface atoms. Some behavioral similarities that exist between the N-BK7 plasma etching and thermal oxidation of silicon are the reason for the choice of this model. It was shown that the plasma etching of N-BK7, like thermal oxidation of silicon, is accomplished through three different phases that the plasma-generated fluorine atoms undergo, including diffusion from the surrounding gas to the surface, diffusion through the existing layer to the residue–substrate interface, and interactions with the substrate.

On the basis of this inspiration, a mathematical model that results in a simple formula was developed for the prediction of the plasma etching of N-BK7. This model can describe the relationship between the residual layer thickness and etching time with a very good agreement. The whole process is contained in two so-called DG parameters, which were estimated from experimental data derived by the static etchings for different dwell times.

These model parameters were determined as a function of radial distance, as the plasma-generated fluorine flux has a spatio-temporal distribution. By the estimation of the lateral distributions of the residual layer and etching depth, it was proved that the local etching depth is equivalent to the thickness of the residual layer. Finally, the derived model was extended into the dynamic etching, such as line and area etching of N-BK7, and the outcomes were compared with the experimental results. By introducing such a model, it is possible to account for the effect of the residual layer and surface temperature to predict the growth of etching depths over dwell time. The results lead to a better understanding of the plasma–surface interactions of N-BK7 and help to develop a predictable machining process for plasma-based freeform generation.

The applicability of this model to other optical glasses will be investigated in the future to extend the machining capabilities using plasma jet etching. Furthermore, the underlying processes of layer formation, the evolution of porosity of the residual layer, and connected diffusion and reaction mechanism require a detailed clarification.

ACKNOWLEDGMENTS

The partial financial support by the German Federal Ministry of Education and Research (BMBF) within the framework of the InnoProfile-Transfer initiative 03IPT706X “Ultra-precision manufacturing using atomic particle beams” is gratefully acknowledged.

ORCID

Faezeh Kazemi https://orcid.org/0000-0003-2974-0726

REFERENCES

[1] H. Takino, K. Yamamura, Y. Sano, Y. Mori, *Appl. Opt.* **2010**, *49*, 4434.

[2] Y. Mori, K. Yamamura, K. Yamauchi, K. Yoshii, T. Kataoka, K. Endo, K. Inagaki, H. Kakiuchi, *Nanotechnology* **1993**, *4*(*4*), 225.

[3] Y. Mori, K. Yamamura, Y. Sano, *Cryst. Growth Technol.* **1993**, 1993.

[4] Y. Mori, K. Yamamura, Y. Sano, *Rev. Sci. Instrum.* **2000**, *71*(*12*), 4620.

[5] R. Jourdain, M. Castelli, P. Shore, P. Sommer, D. Proscia, *Prod. Eng. Res. Dev.* **2013**, *7*, 665.

[6] M. Castelli, R. Jourdain, P. Morantz, P. Shore, *Precis. Eng.* **2012**, *36*(*3*), 467.

[7] Y. Verma, A. K. Chang, J. W. Berrett, K. Futtere, G. J. Gardopee, J. Kelley, T. Kyler, J. Lee, N. Lyford, D. Proscia, P. R. Sommer, *Proc. SPIE* **2006**, *6273*, 62730.

[8] L. Na, X. Qiang, Z. Peng, W. Bo, *Plasma Sci. Technol.* **2015**, *17*(*7*), 567.

[9] B. Shi, Y. Dai, X. Xie, S. Li, L. Zhou, *Plasma Chem. Plasma Process.* **2016**, *36*(*3*), 891.

[10] H. Paetzelt, G. Boehm, T. Arnold, *Plasma Sources Sci. Technol.* **2015**, *24*, 025002.

[11] T. Arnold, G. Boehm, R. Fechner, J. Meister, A. Nickel, F. Frost, T. Haensel, A. Schindler, *Nucl. Instrum. Methods Phys. Res., Sect. B* **2010**, *616*, 147.

[12] T. Arnold, G. Boehm, H. Paetzelt, *J. Eur. Opt. Soc. -Rapid* **2016**, *11*, 16002.

[13] C. F. Cheung, L. Kong, M. Ren, D. Whitehouse, S. To, *CIRP Ann.* **2012**, *61*(*1*), 527.

[14] Y. Jingfei, L. Chen, X. Li, Q. Yuan, Z. Gao, *NASA Astrophysics Data System (ADS)* **2017**, *11*, 01.

[15] D. Walker, G. Y. Yu, C. Gray, P. Rees, M. Bibby, H. Y. Wu, X. Zheng, *Adv. Mater. Res.* **2016**, *1136*, 684.
[16] J. A. Menapace, P. J. Davis, W. A. Steele, M. R. Hachkowski, A. Nelson, K. Xin, *Proc. SPIE* **2007**, *6403*, 6403.
[17] R. Pan, B. Zhong, D. Chen, Z. Wang, J. Fan, C. Zhang, S. Wei, *Int. J. Mach. Tool Manufact.* **2018**, *124*, 43.
[18] J. Meister, T. Arnold, *Plasma Chem. Plasma Process.* **2010**, *31*, 91.
[19] F. Kazemi, G. Boehm, T. Arnold, *Proc. Optics and Measurement International Conference, Czech Republic. 2019*. International Society for Optics and Photonics: Pergamon Press **2019**, 11385.
[20] B. E. Deal, A. S. Grove, *J. Appl. Phys.* **1965**, *36*(*12*), 3770.
[21] G. Gerlach, K. Maser, *Adv. Condens. Matter Phys.* **2016**, *13*, 7545632.
[22] M. A. Hopper, R. A. Clarke, Young, *J. Electrochem. Soc.* **1975**, *122*(*9*), 1216.
[23] F. Kazemi, G. Boehm, T. Arnold, *Plasma Process. Polym.* **2020**, *17*, 8.
[24] F. Kazemi, G. Boehm, T. Arnold, *Plasma Process. Polym.* **2019**, *16*, 12.
[25] D. Gray, I. Tempermeister, H. Sawin, *J. Vac. Sci. Technol., B* **1993**, *11*, 4.
[26] H. Chae, *J. Korean Phys. Soc.* **2007**, *51*(*3*), 978.

How to cite this article: Kazemi F, Boehm G, Arnold T. A novel Deal–Grove-inspired model for fluorine-based plasma jet etching of borosilicate crown optical glass. *Plasma Process Polym*. 2021;18:e2000218. https://doi.org/10.1002/ppap.202000218